Using a Co-located GNSS Radio Occultation Payload for Microwave Radiometer Calibration
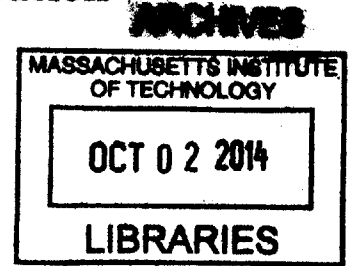
by

Pratik K. Dave

B.S. Aerospace Engineering
University of Maryland, 2009

Submitted to the Department of Aeronautics and Astronautics
in partial fulfillment of the requirements for the degree of

Master of Science in Aeronautics and Astronautics

at the

MASSACHUSETTS INSTITUTE OF TECHNOLOGY

June 2014

Signature redacted

Author . . . .
Department of Aeronautics and Astronautics
May 22, 2014

Signature redacted

Certified by . . . .
Kerri Cahoy
Assistant Professor of Aeronautics and Astronautics
Thesis Supervisor

Signature redacted

Accepted by . . . .
Paulo C. Lozano
Associate Professor of Aeronautics and Astronautics
Chair, Graduate Program Committee

Using a Co-located GNSS Radio Occultation Payload for Microwave Radiometer Calibration

by

Pratik K. Dave

Submitted to the Department of Aeronautics and Astronautics
on May 22, 2014, in partial fulfillment of the
requirements for the degree of
Master of Science in Aeronautics and Astronautics

Abstract

This study presents a new method of calibrating an orbital cross-track scanning microwave radiometer using a co-located radio occultation (RO) instrument with Global Navigation Satellite Systems (GNSS). The radiometer and RO receiver periodically observe the same volume of atmosphere near the earth's limb, allowing for overlapping, or collocated, measurements that can be used to calibrate the radiometer. This method leverages the benefits of both remote sensing techniques to strengthen the science returned with the goal of achieving dense geospatial sampling and highly accurate calibration. Performance analyses show that the technique is particularly well-suited for implementation on a low-cost CubeSat hosting both radiometer and RO receiver systems on the same spacecraft. We describe a validation platform for this calibration method, the Microwave Radiometer Technology Acceleration (MiRaTA) CubeSat, currently in development by MIT Lincoln Laboratory and MIT Space Systems Laboratory for the NASA Earth Science Technology Office. MiRaTA will fly a multi-band radiometer and the Compact TEC/Atmosphere GPS Sensor (CTAGS) in 2016. We investigate the effect of system design parameters such as hardware specifications and operational concepts on the performance of this co-located remote sensing method.

Thesis Supervisor: Kerri Cahoy
Title: Assistant Professor of Aeronautics and Astronautics

Acknowledgments

First and foremost, I would like to thank Dr. Kerri Cahoy (Massachusetts Institute of Technology, Department of Aeronautics and Astronautics) and Dr. William J. Blackwell (MIT Lincoln Laboratory) for their technical guidance and support over the course of this research.

Thanks to the MIT Lincoln Laboratory for their generous financial support through the Lincoln Scholars Program, which enabled my graduate education and this research.

Thanks to Annie Marinan, Eric Peters, Evan Wise, Kerri Cahoy, Meghan Quadrino, and Ryan Kingsbury for the considerable assistance and entertainment you provided as we all pushed MicroMAS to completion, along with the rest of the MicroMAS team for the environment and facilities to do so.

Finally, many thanks to Mom, Dad, Stuti, Parvish, Orion, and numerous friends and family that provided me with encouragement or mental/physical escape whenever I needed it.

Contents

List of Figures

List of Tables

Chapter 1

Introduction

1.1 Motivation

On the 29th of October 2012, Hurricane Sandy made landfall in New Jersey and continued a destructive path into the record books, becoming the second-costliest hurricane in United States history [11]. Studies by the US National Oceanic and Atmospheric Administration (NOAA) and the European Centre for Medium-range Weather Forecasts (ECMWF) have shown that data from polar-orbiting weather satellites were key in predicting Sandy's US-bound track several days in advance of landfall [23, 24]. When the polar-orbiting satellite data were removed from the models, the storm was predicted to remain at sea and not take the sudden "left hook" toward the US coast. The advance warning provided by the assimilated data proved critical towards giving authorities and residents in coastal states time to prepare for the storm.

Current polar-orbiting missions that actively provide meteorological data include the Polar Operational Environmental Satellites (POES) mission co-led by NOAA and the European Organisation for the Exploitation of Meteorological Satellites (EU-METSAT), the Defense Meteorological Satellite Program (DMSP) mission led by the US Department of Defense (DoD), and a number of science missions led by international space agencies, such as the Earth Observation System (EOS) mission led by the US National Air and Space Adminstration (NASA). One of the advantages

of polar-orbiting satellites is that they provide the meteorological community with accurate temperature and water vapor data at high spatial and temporal resolution [24].

Table 1.1: Operational Polar-orbiting Weather Satellites, as of May 2014 [26]

Operational Satellite	Agency	Equatorial Crossing Time (train)	Microwave Instruments	Launch Year	Expected EOL
DMSP-F16	DoD	05:22 (early AM)	SSMIS	2003	$\geq$ 2014
DMSP-F19	DoD	05:30 (early AM)	SSMIS	2014	$\geq$ 2019
DMSP-F17	DoD	05:49 (early AM)	SSMIS	2006	$\geq$ 2014
DMSP-F18	DoD	08:06 (morning)	SSMIS	2009	$\geq$ 2014
Metop-A	EUMETSAT	09:30 (morning)	AMSU-A MHS	2006	$\geq$ 2014
Metop-B	EUMETSAT	09:30 (morning)	AMSU-A MHS	2012	$\geq$ 2018
Suomi-NPP	NOAA, NASA	13:25 (afternoon)	ATMS	2011	$\geq$ 2016
NOAA-19	NOAA	13:39 (afternoon)	AMSU-A MHS	2009	$\geq$ 2014
NOAA-18	NOAA	15:23* (afternoon)	AMSU-A MHS	2005	$\geq$ 2014

A single polar-orbiting satellite is able to achieve repeating global coverage every 12 hours, thus providing numerical weather prediction (NWP) centers with refreshed data twice per day. Current polar-orbiting efforts enhance this capability by employing a constellation architecture of three coordinated polar-orbiting trains that repeat groundtracks approximately every 4 hours, thus allowing NWP updates several times per day. As seen in Table 1.1, POES spacecraft are distributed such that EUMETSAT fills the "morning" train, while NOAA fills the "afternoon" train approximately four hours after the morning orbit. The DMSP spacecraft primarily fills an "early-morning" train approximately four hours earlier than the morning orbit.

Several operational data gaps are projected in the polar-orbiting weather satellite

architecture. While EUMETSAT is on-track with the development of additional satellites to ensure continued data-collection from the morning orbit, at least a year-long gap is projected in the afternoon orbit beyond 2016, when the current NOAA spacecraft will have reached the end of their designed lifetimes. The next-generation of NOAA spacecraft, called the Joint Polar Satellite Systems (JPSS) mission, will not be ready until 2017. This gap could grow larger either if the current satellite fails earlier than planned, or the first JPSS satellite incurs any delay in launch readiness [21]. Another data gap is projected in the early-morning orbit beyond 2020, when the current DMSP spacecraft will have reached the end of their designed lifetimes. There are currently no funded DoD weather satellite missions beyond 2020, when the final DMSP satellite is slated to launch, leaving the early-morning orbit without a dedicated operational spacecraft [2, 26]. Each gap results in reduced quantity and timeliness of data, leading to diminished NWP and tropical storm monitoring capabilities.

The risks that these data gaps pose to the state of global NWP and tropical storm monitoring have raised major concerns across the meteorological community. However, the substantial costs associated with developing traditional multi-instrument weather satellites stands in the way of simply launching more operational satellites in order to alleviate the data concerns. For instance, NOAA's most recent polar-orbiting weather satellite, Suomi-NPP, launched in 2011 as the bridge between POES and JPSS with a development life-cycle cost close to $900 million [25].

One potential way to mitigate high development costs is to shift towards small-satellite designs, which are becoming increasingly capable of accomplishing Earth-observation mission objectives that formerly required larger and more expensive platforms [22]. The following sections highlight two remote-sensing techniques, passive microwave radiometry and GNSS radio occultation, that can be incorporated into a small-satellite constellation architecture in order to assist in both the improvement of tropical storm monitoring, and the mitigation of numerical weather prediction data gaps.

15

1.2 Passive Microwave Radiometry

Impact studies on tropical storm forecasting have shown that passive microwave radiometer measurements contribute most towards reducing forecast errors, as seen in Fig. 1-1. Microwave radiometers (MWRs) sense atmospheric and terrestrial radiation in the 1-1000 GHz frequency band, enabling cloud-penetrating, all-weather observation that meteorological instruments in the visible and infrared ranges cannot achieve. Meteorological applications supported by MWRs include climate monitoring profiles of temperature and humidity, precipitation measurements, and cloud observations.
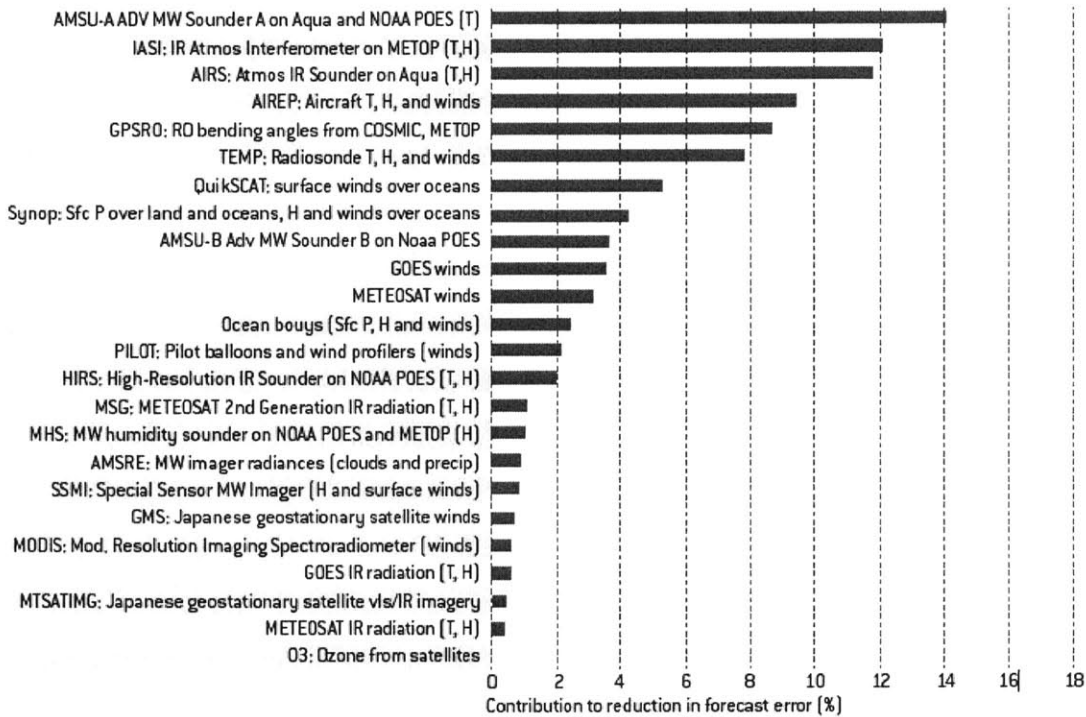
Figure 1-1: Chart of remote sensing instruments prioritized based on their contribution in reducing forecast errors [3]

1.2.1 Notable Missions

The current state-of-the-art microwave radiometer is the Advanced Technology Microwave Sounder (ATMS) on the Suomi-National Polar-Orbiting Partnership (Suomi-

16

NPP) satellite, launched in 2011. The ATMS instrument improves upon the legacy of a long line of notable microwave sounding instruments dating back to the Microwave Sounding Unit (MSU), first launched in 1979, followed by the Advanced Microwave Sounding Unit (AMSU) series of instruments, first launched in 1998 and currently flying on the Metop 1st-generation satellites and NOAA 5th-generation satellites. ATMS has been shown to achieve on-orbit radiometric accuracies <1.0 K [17].

Three CubeSat-class demonstrations of microwave instruments are planned for launch/deployment in the next year, including the MIT Micro-sized Microwave Atmospheric Satellite (MicroMAS) mission [8], the JPL/UT-Austin Radiometer Atmospheric CubeSat Experiment (RACE) mission [20], and the UC-Boulder PolarCube [14] mission. These demonstrations preview the capability of performing passive microwave radiometry from a nanosatellite constellation.

1.2.2 Calibration Problem

Additional MWRs in additional low-earth orbit (LEO) planes could further improve the achievable spatial and temporal resolutions [22], though regular calibration of the sensor is necessary in order to remove biases and achieve better accuracies. To calibrate a microwave sensor, two or more sources of known radiation must be regularly observed. Observing deep space provides a cold reference point, as the observed brightness temperature of the cosmic background has a known relationship to the observing channel frequency. In order to provide one or more warm reference points such that the sensor calibration gain can be derived over a range of observed brightness temperatures, internal calibration targets (ICTs) are used in traditional scanning microwave instrument designs. However, ICTs have high demands on spacecraft size, weight, and power (SWaP), impacting the overall size and cost of the satellite design.

The MicroMAS mission, to be launched in mid-2014, aims to resolve this limitation by reducing the SWaP demands of a single-band (118 GHz) microwave radiometer instrument such that the payload can be accommodated along with the supporting subsystems into a three-unit CubeSat structure [7]. In place of ICTs, the MicroMAS payload utilizes noise diodes to provide the warm reference points needed to derive

17

the calibration gain. However, this solution is best suited to short-duration missions like the proof-of-concept MicroMAS mission, as noise diode biases are known to drift over time [12]. Operational missions with durations longer than a few months would require an accurate secondary calibration source in order to remove the drifting noise diode bias over the mission lifetime.

1.3 GNSS Radio Occultation

Radio occultation measurements have also been used extensively to improve weather forecasting and assessments of climate, as shown in Fig. 1-1. Radio occultation is a technique of measuring the refractivity of planetary atmospheres by calculating the amount that a radio signal is refracted by the atmopshere between a transmitting spacecraft and a receiver. The refraction bending angle is a function of the atmospheric density at the tangent point of the signal path between transmitter and receiver, and can be obtained from the phase delay in the signal [18]. The accuracy of phase delay measurements is highly dependent on knowledge of the signal (e.g. center frequency, bandwidth, stability) and position-knowledge of both the source and receiver. Global navigation satellite systems (GNSS) like the US Global Positioning System (GPS) are designed to provide both signal-knowledge and position-knowledge to a high degree of accuracy, and thus are a useful source for terrestrial radio occultation applications, known as GNSS-RO. Fig. 1-2 depicts the geometry of performing radio occultations. Meteorological applications supported by GNSS-RO include climate monitoring profiles of temperature, pressure, and humidity, and total electron content (TEC) measurements in the ionosphere.

1.3.1 Notable Missions

The current state-of-the-art GNSS-RO mission is COSMIC/FORMOSAT-3, a joint US-Taiwan six-satellite constellation program that has collected over 4,000,000 total atmospheric occultations with the GPS constellation since launch in 2006. Early studies showed a precision between instruments of approximately 0.05 K [1]. The

18
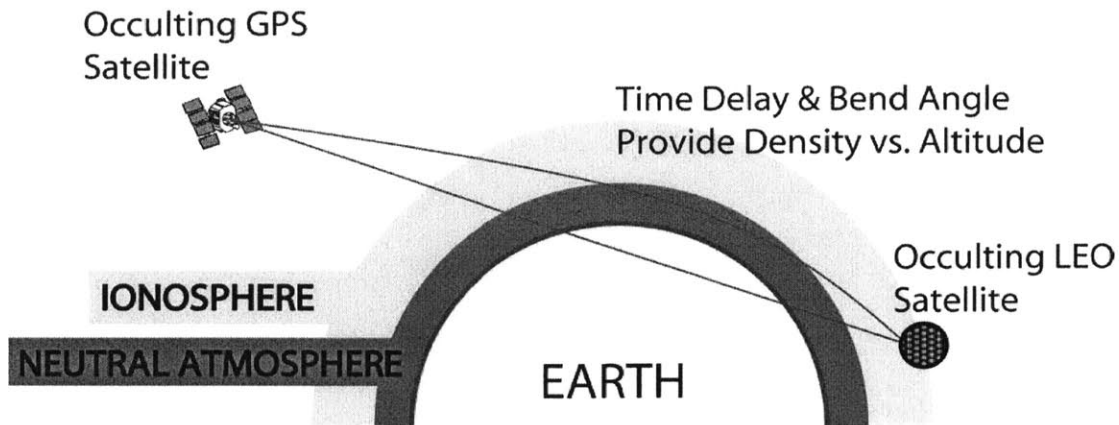
Figure 1-2: Depiction of radio occultation geometry [3]

mission has proven profoundly useful in reducing NWP errors and providing reference data for validations of other remote sensing instruments. Other notable missions include GPS/MET mission, which conducted the first RO measurements of Earth's atmosphere back in 1995 [27], and the GRAS instruments currently flying on the Metop 1st-generation satellites [30].

The US Air Force Pico-Satellite Solar Cell Testbed-2 (PSSCT-2) mission, launched in 2011, aimed to demonstrate several new small-satellite technologies on a nanosatellite platform. Amongst them was the Compact Total Electron Content Sensor (CTECS) radio occultation instrument, developed by The Aerospace Corporation. Using patch-array antennas and compact GPS receiver electronics to reduce the instrument SWaP, CTECS successfully collected TEC and electron density profiles between 60 and 320 km above sea level from an orbital altitude of about 350 km [4]. A CubeSat-class demonstration of a GNSS-RO capable receiver, the UT-Austin ARMADILLO mission, is scheduled for launch in the next year [13]. These demonstrations preview the capability of performing GNSS-RO from a nanosatellite constellation.

1.3.2 Data Density Problem

Although GNSS-RO provides highly accurate data, its spatial and temporal resolution is limited by the number of spacecraft in both the transmitting and receiving

19

constellations. When the COSMIC/FORMOSAT-3 constellation was at peak opera-
tion, it provided approximately 2,000 occultation profiles per day [1]. The follow-on
mission, COSMIC-2/FORMOSAT-7, is projected to achieve up to 12,000 profiles per
day resulting from upgrades in both the transmitting constellation (using additional
signals from Galileo and GLONASS spacecraft) and the receiving constellation (using
an additional 6 spacecraft at a higher inclination) [16]. Though this is an impressive
planned upgrade in the quantity of data collected, is it much less than the 3,000,000
soundings per day achievable by a single polar-orbiting ATMS instrument [9]. Still,
increasing GNSS-RO capabilities should remain a priority as it does not require cal-
ibration and thus provides excellent reference measurements for data validation and
assimilation into NWP models.

1.4   Combination of Remote Sensing Techniques

Considering the complementary advantages of these two remote sensing techniques,
and their shared ability in being performed from small-satellite platforms, it seems
that a synergistic solution can be found by combining passive microwave radiometry
and GNSS radio occultation into a small-satellite constellation architecture in order to
achieve dense, high-accuracy atmospheric sounding. The following sections describe
two potential methods for accomplishing this combination of techniques.

1.4.1   Dual-constellations Method

The dual-constellations method involves deployment of two coordinated small-satellite
constellations, one with MWR payloads and the other with GNSS-RO payloads. A
preview for this concept was shown in a recent study in which RO data from the
COSMIC/FORMOSAT-3 constellation was used to achieve absolute calibration of
collocated[1] ATMS brightness temperature data from Suomi-NPP without any sys-

---

[1]The term "collocate" is used in this thesis in reference to two or more data sets that are matched
within specific bounds of time and spatial volume. It is not to be confused with the term "co-locate"
which is used in this thesis in reference to two or more items which share the same location, as in
two instruments on the same spacecraft.

tematic bias [32].

However, an operational remote-sensing program using a dual-constellation architecture would rely heavily on the ground systems. For example, in the case of a single MWR satellite and a single RO satellite, the ground systems architecture would need to retrieve all of the data from both instruments, isolate sets of collocated data, process the data to determine the MWR bias-corrections, and apply the calibration to the rest of the MWR data before it is passed forward for assimilation into NWP models. When expanded into a constellation architecture, the quantity of data to process would cause quite a burden on ground stations and data-processing centers.

1.4.2   Co-located Payloads Method

Another method would be to deploy a single constellation of small satellites with both MWR and GNSS-RO instruments, which has the potential to be both simpler and cheaper than a dual-constellation concept. A study recently conducted by EUMETSAT, which conveniently has both MWR and GNSS-RO payloads on their Metop satellites, concluded that the use of collocated RO data to calibrate microwave sounders on the same spacecraft has profound potential for long-term atmopsheric monitoring campaigns [19].

As with any remote-sensing constellation effort, this co-located payloads approach would still demand improved processing capabilities in ground systems as the number of satellites increases. However, this problem can be alleviated slightly if a portion of the data architecture could be shifted from ground processing to on-board processing, a feature of co-located payloads that is not available in the dual-constellations architecture without inter-satellite communications. The data collocation, processing, and calibration operations could all be performed on-board the spacecraft, reducing both the amount of data needed to be retrieved by ground stations, and eliminating the amount of processing needed before the data is assimilated into NWP models. This thesis investigates a procedure for calibrating a passive microwave radiometer using data from a co-located GNSS radio occultation payload.

21

1.5 Research Outline

The research discussed in this thesis follows two goals:

1. To identify a potential calibration procedure for calibrating a passive microwave radiometer using data from a co-located GNSS radio occultation payload

2. To analyze the performance of the proposed calibration procedure, both in terms of accuracy and sensitivity to some critical system parameters

Chapter 2 outlines the approach to achieving these research goals by defining the proposed calibration procedure, and describing the simulation environment that was used to analyze the calibration procedure's performance. Chapter 3 focuses on the results of the simulations conducted to analyze the accuracy of the calibration procedure, while Chapter 4 focuses on the results of those analyzing its sensitivity to the orbital altitude of the system, the beamwidth of the radiometer, and the sampling rate of the radiometer. Chapter 5 summarizes the findings of this research.

1.5.1 Future Validation with the MiRaTA Mission

The MIT Microwave Radiometer Technology Acceleration (MiRaTA) mission, to be launched in 2016, aims to validate the concept of co-locating microwave radiometer and GNSS radio occultation payloads on a small satellite platform. The proposed radiometer, designed by MIT Lincoln Laboratory and UMass-Amherst, improves on the heritage MicroMAS radiometer design by using three frequency bands: 52-58 GHz for temperature sounding, 175-191 GHz for water vapor sounding, and 206.4-208.4 GHz for cloud ice sensing. The proposed Compact TEC/Atmosphere GPS Sensor (CTAGS) radio occultation payload, designed by The Aerospace Corporation, will improve upon the CTECS design by featuring a multi-patch antenna array to collect occultation observations into the lower atmosphere, down to at least 20 km altitude. Both payloads will be assembled into a three-unit CubeSat structure along with the accompanying avionics, power, thermal, and attitude determination/control subsystems [8].

Top View

velocity vector

10x10x34 cm
4.0 kg

Bottom View
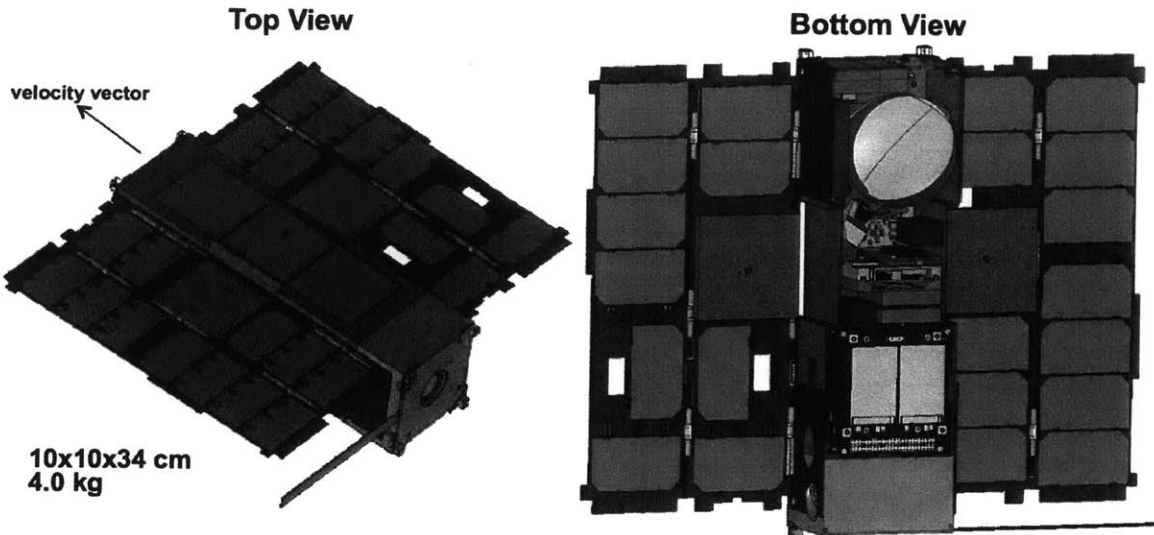
Figure 1-3: CAD drawing of proposed MiRaTA spacecraft concept [9]

Fig. 1-3 shows a CAD drawing of the preliminary MiRaTA spacecraft concept. A view looking down onto the top of the MiRaTA spacecraft is shown on the left, and a view of the bottom of the spacecraft (with the bottom body panel removed for illustration) is shown on the right. The five-element antenna patch array on the zenith deck of the spacecraft is used for the atmospheric GPSRO measurements. The side patches are integrated onto deployable solar panels (mounted beneath the substrate). The primary spacecraft components are visible in the image on the right, including (from the bottom up): three-axis reaction wheel assembly, avionics and power stack (batteries visible), GPS receivers (two), and radiometer components. The side patch antennas fold inwards and occupy a fraction of space along the body panels of the spacecraft prior to deployment. The cutouts in the deployed solar panels allow access to spacecraft electronics. A representative UHF tape-spring antenna is shown for illustration purposes - the flight version will likely be positioned on the lower deck of the spacecraft to permit the use of a larger ground plane.

It is important to note, that a shift in the data architecture for a given mission (from ground to on-board processing) has a significant impact on the overall system design, placing different requirements primarily on the avionics and flight-software subsystems, which would undoubtedly flow into the other supporting subsystems.

23

Therefore, a mission with the objective of performing on-board radiometer calibration using a co-located RO instrument would need to be specifically designed to the task.

The MiRaTA spacecraft is not planned such that the data collocation, processing, and calibration operations can be performed on-board the spacecraft. However, the mission does plan to collect collocated MWR and RO data such that a radiometer calibration procedure using data from a co-located GNSS-RO payload can potentially be demonstrated on the ground for use in future missions. As such, the MiRaTA mission is the validation platform for the research presented in this thesis, and thus serves as the basis for the system design assumptions used in the analyses.

Chapter 2

Approach

This chapter focuses on the approach used in order to propose a method for calibrating microwave radiometer observations using radio occultation profiles from colocated instruments. Section 2.1 defines the calibration procedure, noting relevant data processing algorithms and retrieval methods. Section 2.2 describes the simulation environment used in this study to analyze the performance of the calibration procedure.

2.1 Proposed MWR Calibration Procedure using Co-located GNSS-RO

2.1.1 Background on Microwave Radiometers

A passive microwave radiometer measures the amount of radiant intensity, or radiance, received in a given microwave frequency band, f, from objects in the instrument's field-of-regard. Radiant intensity, I, is often expressed in terms of an equivalent brightness temperature, T_B, via the Rayleigh-Jeans equation [15]:

$$T_B = \frac{c^2}{2f^2 k} I \tag{2.1}$$

where c is the speed of light, f is the sensing channel frequency, and k is the Boltzmann constant. The radiation is received via the reflector antenna (henceforth referred to as the "reflector", in order to differentiate from the RO antenna), and then passed through a mixer that combines the raw signal with an AC voltage source and outputs to an amplifier. The amplified signal is mixed into the frequency bands of interest and squared by a semiconductor diode. Each signal is then introduced to a low pass filter that removes high frequency disturbances and finally converted into digital signals via an analog-to-digital (A/D) converter. Additional details on the design and analysis of microwave radiometers can be found in [29].

The purpose of calibrating a microwave radiometer is to determine the radiometer gain, g. The gain represents the instrument's systematic translation of radiometer "counts," or the digital number output from the A/D converter, into observed brightness temperature, and is thus measured in units of Kelvin/count. The gain value can be determined during pre-launch ground testing on the instrument, however this pre-determined value would not account for any systematic changes in the instrument that may occur during launch (due to vibration or atmopsheric change) or on-orbit (due to temperture fluctuations, external radiation interference, or general degradation). For this reason, calibration must also occur during post-launch validation and regularly during on-orbit operations [31]. Both pre-launch and post-launch calibrations are generally performed using a two-point technique.

2.1.2 Radiometer Brightness Temperature Calibration using a Two-point Algorithm

Brightness temperature calibration is performed by measuring the radiometer count output when reference targets of known brightness temperatures are placed in the radiometer's field-of-regard. For two-point calibration, a minimum of two measurements would be taken – one at a cold reference point, and one at a hot reference point

– and the radiometer gain would be found using the following expression:

$$g = \frac{(T_B - T_{B,c})}{(DN - DN_c)} \tag{2.2}$$

where $T_{B,c}$ and DN_c are the brightness temperature and radiometer count output (digital number) when viewing a cold reference target, and T_B and DN are the brightness temperature and radiometer count output when viewing a warm reference target. However, a more accurate estimation of the radiometer gain can be made by observing the radiometer counts at multiple "warm" reference points that span between the cold and hot brightness temperatures. The radiometer gain can then be determined in using a minimization algorithmn.

Once the gain is determined, it can be used to derive calibrated radiometer brightness temperature measurements, expressed as follows:

$$\tilde{T}_B = \hat{g}(DN - DN_c) + T_{B,c} \tag{2.3}$$

using the same values for $T_{B,c}$ and DN_c as before, and the newly determined radiometer gain $\hat{g}$, along with new DN measurements.

For on-orbit calibrations, the cosmic microwave background radiation conveniently serves as a cold reference point at ∼3 K for remote-sensing microwave radiometers. Warm reference points are thus chosen between 3 K and ∼300 K, the maximum microwave brightness temperature of Earth from orbit. Instead of using high-SWaP internal calibration targets to provide the warm reference points, this study explores the use of measurements from a co-located GNSS-RO payload.

2.1.3 Properties of Collocated Data

In order for a direct comparison to be made between the microwave radiometer count measurements and the RO measurements, the radiometer and GNSS-RO payloads must observe the same column of atmosphere above the earth surface within a given spatial and temporal volume. In section 1.4, two studies regarding the use of collo-

cated data to achieve microwave radiometer calibration were mentioned. The first study compared ATMS data from the Suomi-NPP satellite to RO data from the COSMIC/FORMOSAT-3 constellation, using collocation criteria set by a horiztonal spatial separation of 50 km, and a temporal separation of 180 minutes [32]. The second study compared AMSU-A data to RO data from the GRAS instrument on-board the same Metop satellite, using two cases of collocation criteria. The first was set by a horiztonal spatial separation of 50 km, and a temporal separation of 30 minutes, while the second loosened the criteria a bit, set by a horiztonal spatial separation of 300 km, and a temporal separation of 180 minutes [19]. A key assumption made in this thesis is that the data is perfectly collocated in both the spatial and temporal separations.

2.1.4 Limb-sensing Method for Collecting Collocated Data

Collocated data between the microwave radiometer and GNSS-RO payload can be achieved in a few ways. A nadir-sounding method was used in the MetOp study from 2012 [19]. An important thing to note, however, is that the MetOp satellites are not designed to maximize collocation of data between instruments, but instead designed to maximize the data collection of each instrument individually. Radiometers maximize the spatial resolution of their soundings in a cross-track scanning configuration, while GNSS-RO payloads maximize the quantity and duration of occultations in an along-orbit array configuration. This restricts the collocation of data to the nadir-view of the radiometer during its cross-track scan as it flies over the same "column of atmopshere" that was (or will be) observed by the GNSS-RO payload during a foreward (or aft) occultation event. This method provides a limited quantity of DN measurements that can be compared to the RO measurements per collocation event, since the vertical resolution of MWR nadir-sounding measurements is on the order of 100-times coarser than GNSS-RO measurements [1]. The range of measurements is also limited, since the nadir-view will only observe brightness temperatures between approximately 150 and 300 K.

A limb-sounding method would improve upon these limitations by utilizing entire

radio occultation profiles as opposed to a limited set of measurements at a coarse vertical resolution [5, 10]. RO profiles inherently observe the limb atmosphere, which spans a wide dynamic range between the cold brightness temperature of the cosmic microwave background radiation (~3 K) and the warm brightness temperatures of Earth (~300 K). A system design that allows the microwave radiometer to observe the limb atmosphere at a time before, during, or after the RO collection opportunity (depending on how the system is designed) would not only improve the dynamic range of the collocated measurements, but also the quantity. For these reasons, this thesis analyzes the performance of the limb-sounding method of data collocation.
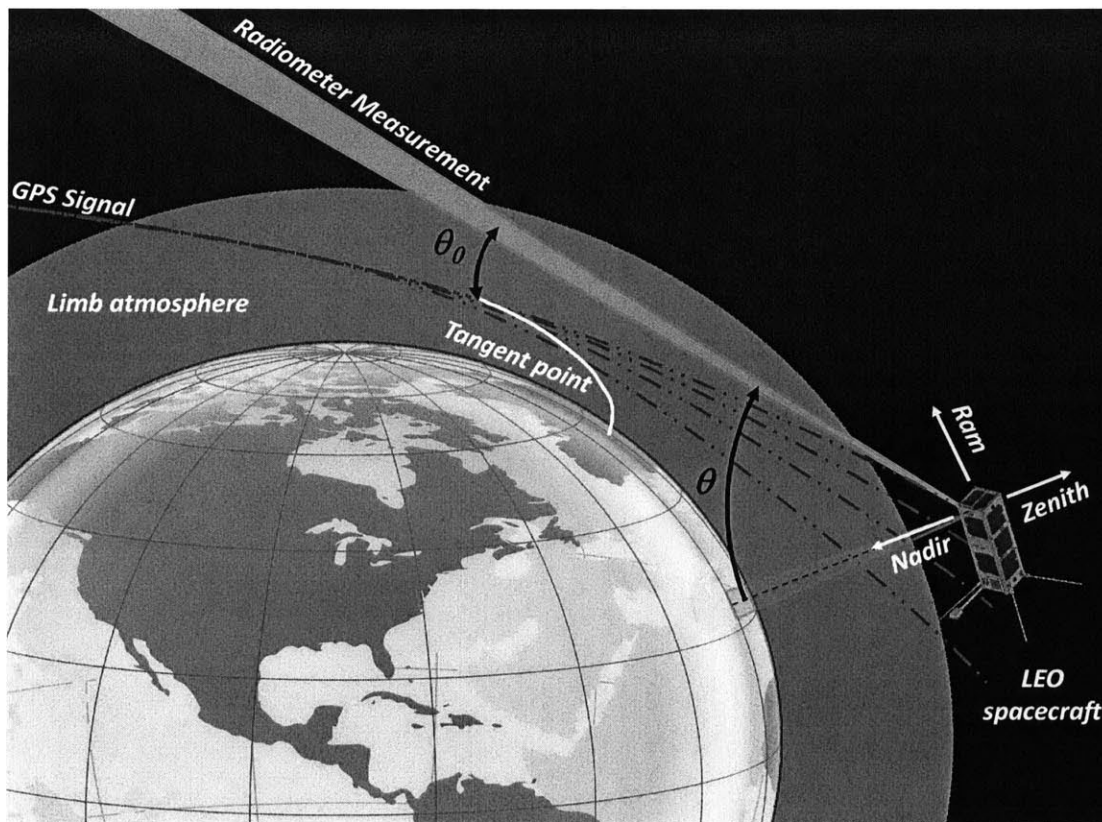

Figure 2-1: Conceptual drawing of a limb-sensing radiometer calibration method using a co-located GNSS-RO payload

Fig. 2-1 shows a conceptual drawing for a limb-sensing method of collecting collocated data from the same spacecraft. Key features are emphasized not-to-scale,

such as the radiometer scan angle θ, the GNSS-RO data profile at atmospheric tangent points, and the radiometer pointing error in the scan plane θ_0.

System Designs for Limb-sensing Method of Data Collocation

Depending on the objectives and constraints of a given mission, a trade decision must be made on how to configure the design of the system. For instance, employing a cross-track scanning radiometer maximizes the spatial resolution of the radiometer data, though it would require GNSS-RO antenna arrays also directed towards the cross-track views of the earth limb, reducing the quantity and duration of occultations. On the other hand, employing an along-orbit GNSS-RO configuration maximizes the occultation opportunities, though it would require a radiometer capable of collecting in the along-track configuration, reducing the spatial resolution of the radiometer data. These two cases represent the extremes; innovative mechanisms (e.g. gimbaled payloads) or ConOps (e.g. spacecraft maneuvers) may be employed to fill in the spaces between in order to meet the requirements of a given mission.

MiRaTA System Design for Data Collocation

As mentioned in section 1.5.1, one of the objectives of the MiRaTa mission is to prove the concept of performing collocated MWR and GNSS-RO data collection from the same spacecraft using a limb-sensing concept. However, given the volume and surface area constraints of a three-unit CubeSat, MiRaTA must use an along-track configuration. The system is designed such that a full spacecraft pitch maneuver aligns a nominally nadir-facing radiometer and zenith-facing GNSS-RO antenna array in opposing along-orbit directions. The maneuver will be time-aligned with a pre-determined occultation opportunity, and is planned to be performed approximately once per orbit [8]. Fig. 2-2 depicts the MiRaTA mission concept of operations in order to validate the primary mission.

30
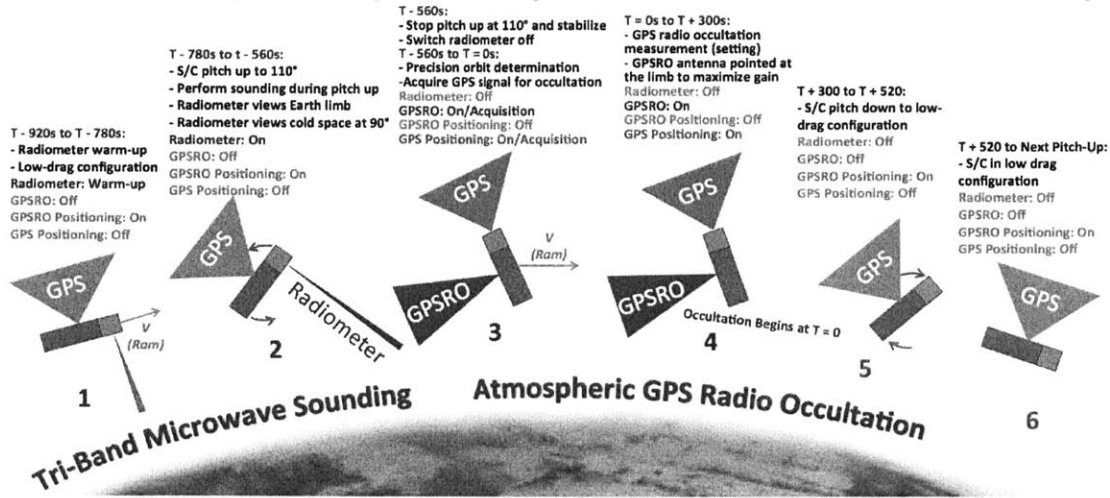
Figure 2-2: Depiction of MiRaTA mission concept-of-operations

2.1.5 Derivation of Brightness Temprature from GNSS-RO Refractivity Profiles

Cross-track scanning microwave radiometers measure the brightness temperature of objects in its field-of-regard as a function of the off-nadir scan angle and channel frequency, $\widehat{T}_B(\theta, f)$. A radio occultation profile yields atmospheric refractivity, from which other atmopsheric properties (e.g. temperature, pressure, moisture) can be derived, as a function of altitude, $N(h)$. In order for these measurements to be used in equation 2.2, the RO refractivity profiles must be transformed into an equivalent microwave brightness temperature. Radiative transfer models, such as those developed by Rosenkranz [28], can be used to transform the RO refractivity profiles into equivalent brightness temperatures, though they are often computationally intensive and need additional inputs that cannot be derived from RO measurements (e.g. ozone content, and surface properties), making them not suited for on-board processing. In this study, a quadratic regression algorithm that maps RO refractivity profiles, $N(h)$ to brightness temperature profiles, $T_B(\theta, f)$, is used instead[1]. This algorithm involves

---

[1]This algorithm was developed by Dr. William J. Blackwell of the MIT Lincoln Laboratory, not by the author. As such, the derivations will not be discussed in this thesis.

two steps. First, the coefficients for an approximate relationship between total transmittance and atmopsheric refractivity are estimated over an ensemble of data, which can be thought of as an on-orbit validation operation. Second, the coefficients for an approximate quadratic relationship between brightness temperature and the total transmittance are estimated over each scan profile. The estimated coefficients are then used to directly relate RO refractivity profiles to brightness temperature profiles for use in calibrating the radiometer data. The accuracy of this approximation algorithm is analyzed in section 3.2.1.

2.2 Simulation Environment

This section describes the simulation environment developed in Matlab in order to analyze the accuracy and performance of the proposed calibration method.

2.2.1 Input Data

The joint MWR and RO calibration process, as defined, has two primary data inputs: (1) the radiometer profile of digital number versus scan angle and channel frequency, $DN(\theta, f)$, and (2) the RO profile of refractivity versus altitude, $N(h)$.

The radiometer profiles were simulated using microwave radiative transfer models temperature developed by Philip W. Rosenkranz [28], and modified slightly[2] to model spherical symmetry and accommodate radiative transfer through the limb atmosphere. The radiative transfer models compute brightness temperature based on atmospheric properties (temperature, pressure, water vapor density, liquid water density, and ozone density), instriument altitude, and channel frequency. A copy resulting brightness temperature profiles $T_B(\theta, f)$ was set aside to be used as the "truth" data for comparison in the performance analyses, while another copy was transformed into radiometer count outputs, $DN(\theta, f)$, using the "true" radiometer gain value of 0.02 Kelvin/count. Finally, noise was introduced into the radiometer counts by feeding

---

[2]Modifications to the software were made by Dr. William J. Blackwell of the MIT Lincoln Laboratory, not by the author. As such, their derivations will not be discussed in this thesis.

random offsets within a 3-counts 1-σ error bounds.

The radio occultation profiles were simulated using the following relationship, adapted from [18]:

$$N = (n - 1) \times 10^6 = 77.6\frac{P}{T} + 3.73 \times 10^5\frac{P_W}{T^2} \qquad (2.4)$$

where n is the index of refraction, P is the atmopsheric pressure, T is the atmospheric temperature, and P_W is the pressure due to water vapor. In this study, the additional terms for electron or moisture content in the atmosphere have been dropped from this relationship. Noise was introduced into the RO data by feeding random offsets within a 0.2% 1-σ error bounds.

2.2.2 Data Sources

The common data source used for both of these inputs is the NOAA88b radiosonde/rocketsonde data set, which contains 7547 global profiles of atmopsheric properties distributed both seasonally and geographically. Details on the characteristics of this data set can be found in [6]. Each profile contains information on the time and location of the data collection along with 100 discrete levels of atmopsheric properties such as temperature, pressure, water and water-vapor content, and ozone content to altitudes exceeding 50 km. In order to emulate collocated data collections, the profiles of both payloads were derived from the same NOAA88b profile.

2.2.3 Output Data

The primary data output of the calibration procedure is calibrated brightness temperature, $\widetilde{T}_B$. This is computed for each discrete combination of profile and channel. Performance results in Chapters 3 and 4 are shown in RMS error for each analyzed channel frequency.

Additional data outputs from the simulation used for analysis include: the estimated radiometer calibration gain, $\hat{g}$; the final residuals from the minimization algorithm (also known as the coefficient of determination, or R^2); the estimated brightness

temperatures from the RO refractivity approximation, $\widehat{T}_B(\theta, f)$; and the estimated angular offset in the representing the spacecraft's pointing error, θ_0.

Chapter 3

Performance of Limb-sounding Calibration Method

This chapter shows and discusses the results from the performance analyses focused on the accuracy of the calibration method for a mission based on the MiRaTA concept. Section 3.1 lists the key notes and assumptions that pertain to the results shown of this study. Section 3.2 shows the results of simulating the limb-sensing method of radiometer calibration. Section 3.3 provides some discussion of the results.

3.1   Key Notes and Assumptions

Of the 7500+ available profiles, 1000 profiles were randomly chosen as inputs to the simulations, ensuring both that the profiles are sufficiently representative of a variety of atmopsheres and locations, and that the simulations could be computed in a reasonable amount of time in order to run multiple performance analyses.

3.1.1   Orbital Altitude

The spacecraft altitude was set to 400 km in this analysis, assuming that MiRaTA will be deployed into orbit from the International Space Station similar to the MicroMAS satellite [8].

Table 3.1: Spectral characteristics of the radiometer channels considered in this study

Channel #	Center Frequency (GHz)	Bandwidth (GHz)	Measurement / Property
1	52.85	600	Temperature
2	53.50	600	Temperature
3	54.15	600	Temperature
4	54.75	600	Temperature
5	55.35	600	Temperature
6	56.65	600	Temperature
7	183.31 ± 1	500	Water vapor
8	183.31 ± 3	1000	Water vapor
9	183.31 ± 7	2000	Water vapor
10	207.4	2000	Cloud ice

3.1.2 Radiometer Characteristics

The performance of the limb-sounding microwave radiometer was analyzed for system design parameters extracted from the preliminary concept for the MiRaTA mission (circa April 2013). As mentioned in section 1.5.1, the MiRaTA radiometer will be designed to observe in multiple frequency bands for temperature, water vapor, and cloud ice measurements. In this study, a total of 10 channels were considered from the proposed frequency bands: six channels from the 50-60 GHz temperature sounding frequency band (hereinafter denoted as "V-band"), and four channels near the 183.31 GHz and 207.4 GHz water vapor sounding bands (hereinafter denoted as "G-band"). The center frequencies and bandwidths of the channels are shown in table 3.1.

The antenna beamwidth (full-width half-maximum, or FWHM) is set to 5.0° for the V-band channels and 1.25° for the G-band channels, as mentioned in the initial MiRaTA proposal. The receiver noise temperatures were assumed to be 300 K and 1000 K, respectively, for the V- and G-bands. For angular spacing requirements, the radiometer is assumed to sample evenly at 0.1° intervals. Fig. 3-1 shows the brightness temperatures of the limb atmosphere as a function of off-nadir scan angle for the channels used in this study.
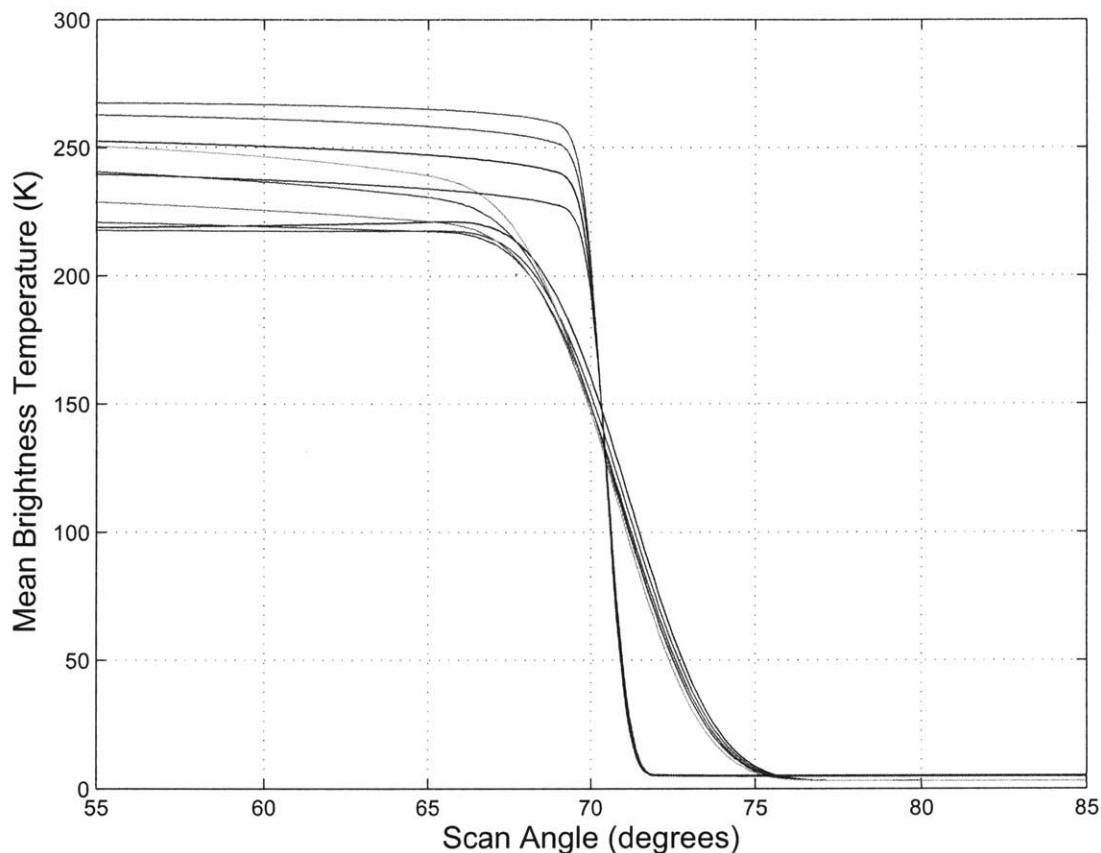
Figure 3-1: Mean brightness temperatures versus scan angle for the proposed MiRaTA radiometer channels (six from the 52-58 GHz temperature sounding band, three from the 183.31 GHz water vapor sounding band, and one at the 207.4 GHz cloud ice sensing band)

3.1.3 Spacecraft Pointing Error

Pointing error due to the spacecraft's attitude determination and control (ADC) subsystem, depicted as θ_0 in Fig. 2-1, was simulated as a random angular offset (with respect to scan angle) in the radiometer profiles used for calibration. Each profile was given a randomized angular offset value. A 1.0° 1-σ error bounds was assumed for the pointing knowledge uncertainty. Since this offset is constant over an entire profile similar to the radiometer gain, the minimization algorithm in the calibration procedure was implemented to retrieve the random angular offsets in addition to the radiometer gain. Pointing error is assumed to have no impact on radio occultation

measurements in this study.

3.1.4   GNSS-RO Payload Capability

Varying capability of the GNSS-RO payload is modeled in the simulation using cutoff altitudes that limit how deep into the limb atmosphere that the payload is able to collect measurements, hereinafter denoted as the RO penetration depth. The calibration procedure was analyzed to five different RO penetration depths: 8 km, 10 km, 12 km, 16 km, and 20 km.

3.2   Results

3.2.1 T_B Approximation

The approximation of radiometer brightness temperatures, $T_B(\theta)$, from RO refractivity profiles, $N(h)$, as described in section 2.1.5, was analyzed for accuracy over the brightness temperature range of 0 K to 250 K. Figs. 3-2 and 3-3 show the performance of the approximation algorithm for the V-band and G-band channels, respectively.

Each sub-figure shows the RMS error in approximating brightness temperature for an individual channel. The colored lines indicate the RO penetration depth used (8 km in blue, 10 km in green, 12 km in red, 16 km in cyan, and 20 km in magenta). In each channel, the lowest errors are achieved in the 8-km case, and the highest errors map to the 20-km case. This is expected, as higher altitudes indicate less data available for use in the estimation of the coefficients in the quadratic relationship between total transmittance and brightness temperature.

These results show that the channel frequency strongly impacts this method of approximating brightness temperatures from the RO refractivity profiles. The 56.65 GHz channel is capable of achieving less than 0.5 K RMS error over the full range of brightness temperatures and for all RO penetration altitude levels, while the results degrade as the channels decrease in transmittance opacity, up to several Kelvin for the G-band channels. This is a important result, as it will impact the performance

38

Figure 3-2: RMS error of the brightness temperature estimation algorithm for V-band temperature sounding channels, where the colored lines indicate the RO penetration depth used (8 km in blue, 10 km in green, 12 km in red, 16 km in cyan, and 20 km in magenta)
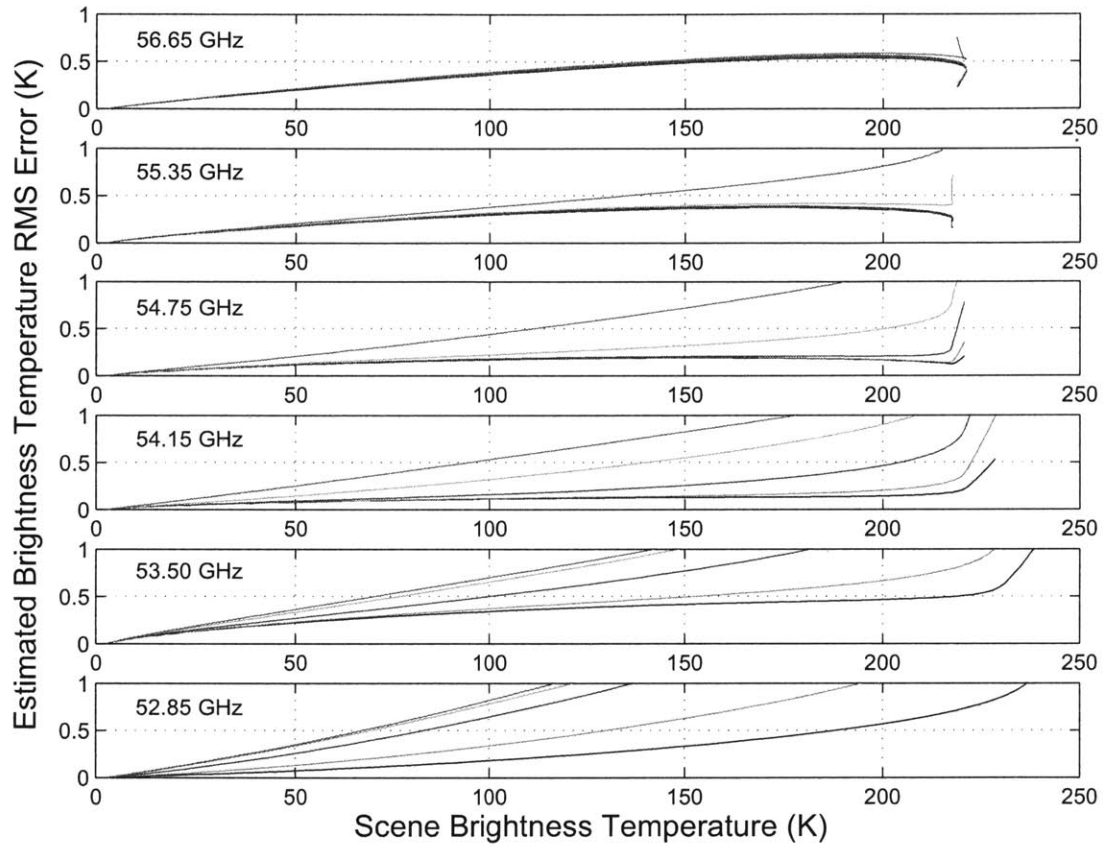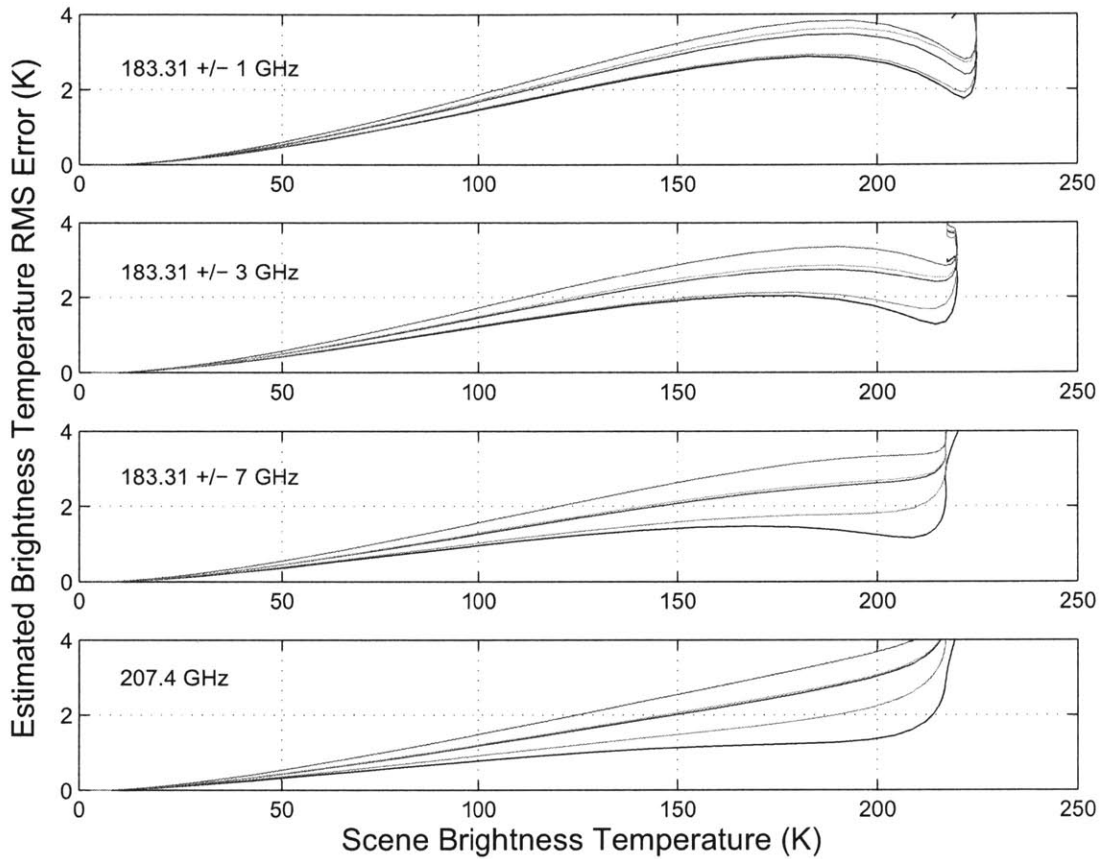
Figure 3-3: RMS error of the brightness temperature estimation algorithm for G-band water vapor sounding channels, where the colored lines indicate the RO penetration depth used (8 km in blue, 10 km in green, 12 km in red, 16 km in cyan, and 20 km in magenta)

of the radiometer calibration algorithm later in the study.

3.2.2 Brightness Temperature Calibration

The results of the proposed limb-sounding calibration algorithm using the RO-derived brightness temperatures are shown in Fig. 3-4. The two plots, one for the V-band channels and one for the G-band channels, show the RMS error of the calibrated brightness temperature after applying the derived radiometer gain to a 300 K scene. Again, each colored line represents a different RO penetration depth between 8 and 20 km.
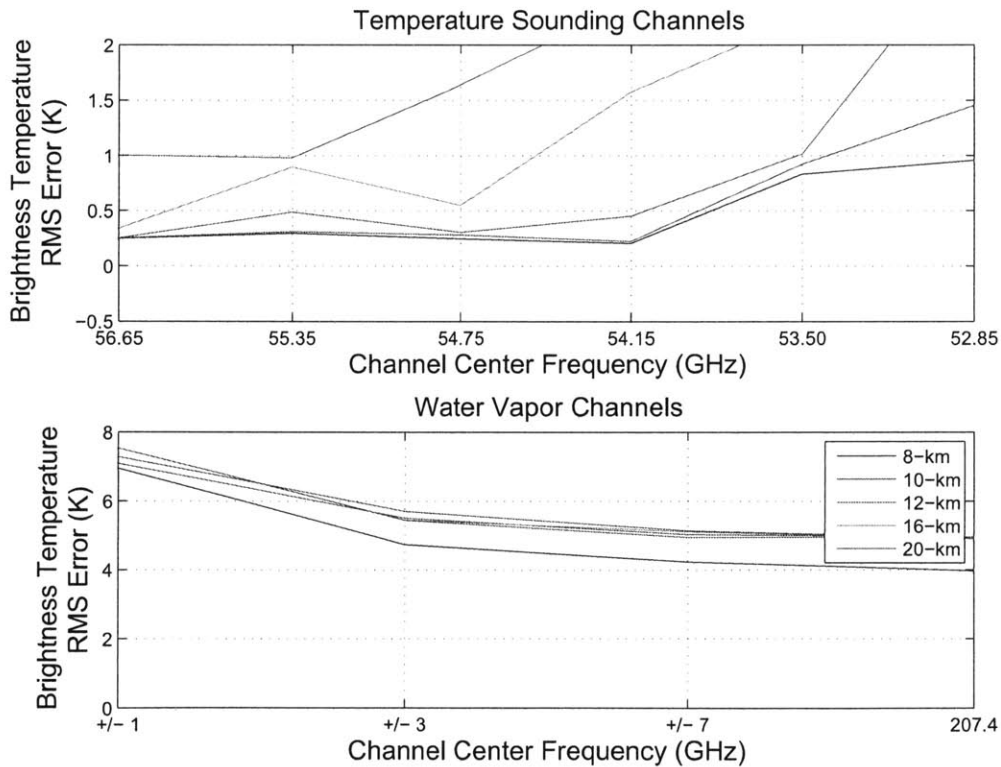

Figure 3-4: RMS error of calibrated brightness temperatures for a 300 K scene, where the colored lines indicate the RO penetration depth used (8 km in blue, 10 km in green, 12 km in red, 16 km in cyan, and 20 km in magenta)

Radiometer calibration using the temperature sounding channels (V-band) shows

promise, as the errors are shown to stay below 1 K for nearly all analyzed frequencies with RO penetration down to 12 km altitude. The results also show a trend of improved performance for more opaque sensing channels. The 56.65 GHz channel achieved the best results with RMS errors below 0.5 K, even with the RO penetration down to the worst-case 20 km altitude. The G-band channels did not perform as well, with errors in the range of 2-6 K. This is likely due to the errors in approximating the radiometer brightness temperature for the less opaque channels, as shown earlier in section 3.2.1. In order to improve the results in these frequencies, approximation relationships that consider moisture would likely need to be developed.
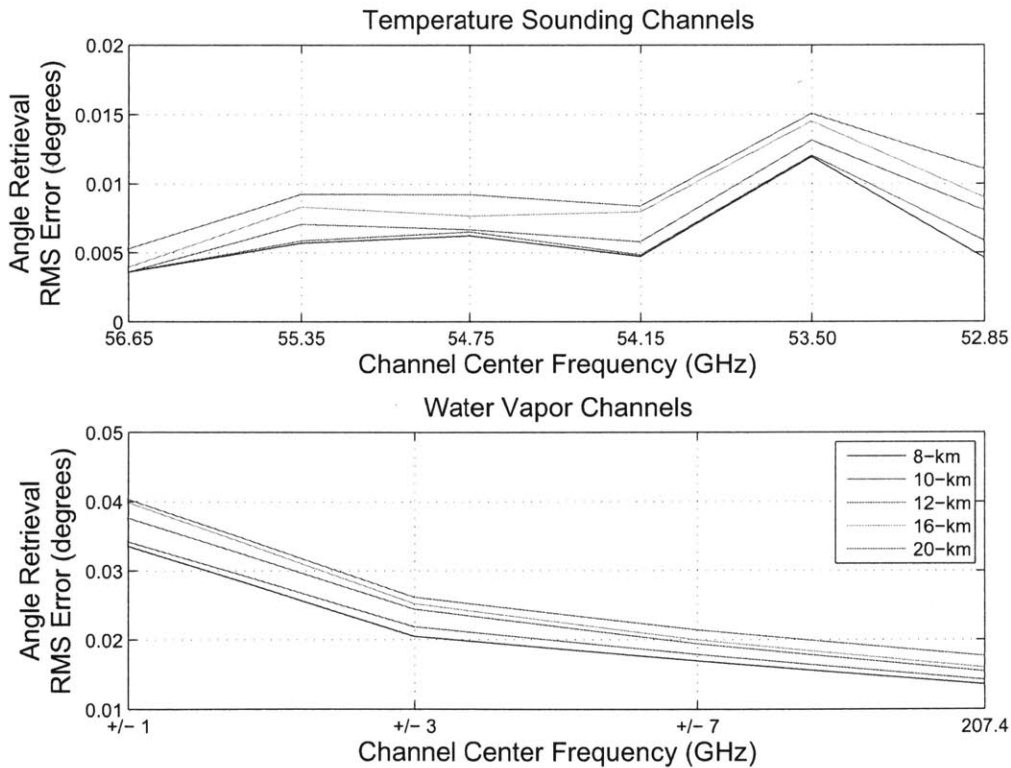

Figure 3-5: RMS error of angle offsets retrieved from observations using the calibration algorithm, where the colored lines indicate the RO penetration depth used (8 km in blue, 10 km in green, 12 km in red, 16 km in cyan, and 20 km in magenta)

42

3.2.3 Angular Offset Retrieval

In addition to the radiometer gain, the random angular offsets simulated between the radiometer and RO profiles were also retrieved as part of the calibration process. The results to the offset retrieval are shown in Fig.3-5. The results are quite good, as accuracies better than 0.05 degrees are achieved for all channels and for all RO penetration depths, reduced from the $1.0°$ $1-\sigma$ errors introduced to the data.
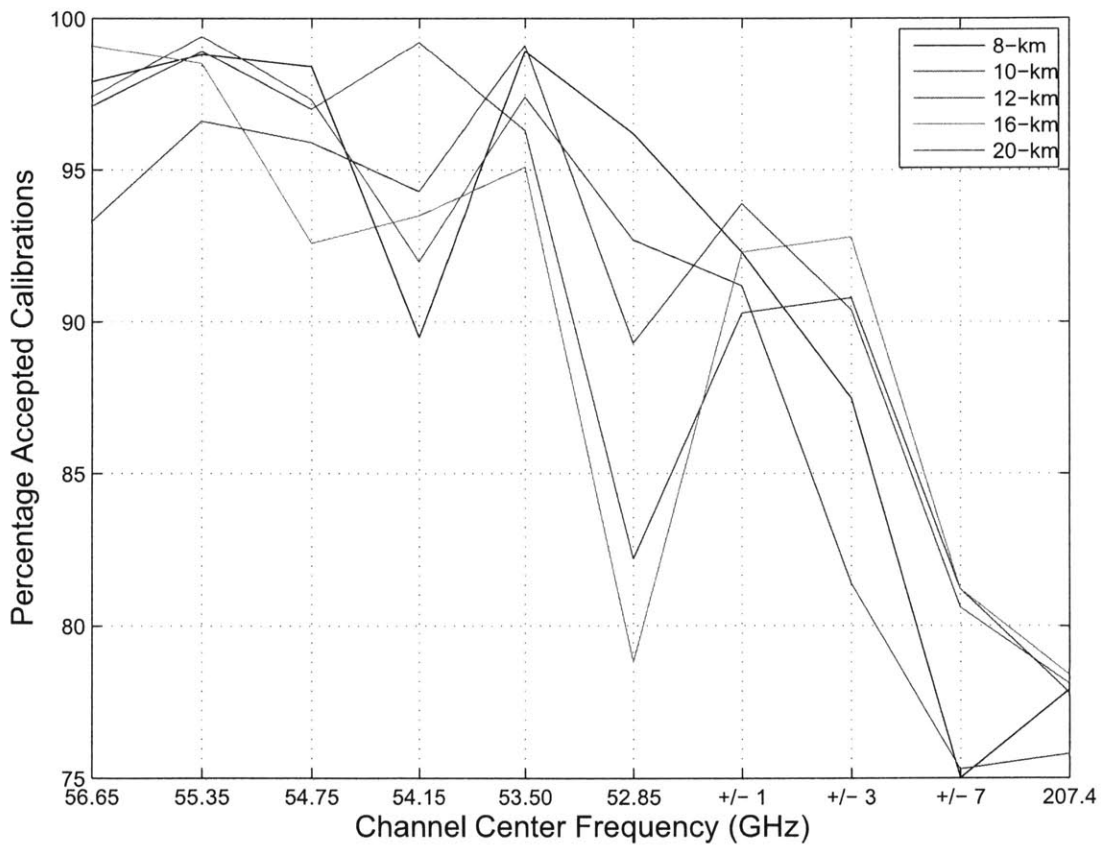

Figure 3-6: Percentage of successful calibrations using the "failure to converge" condition, where the colored lines indicate the RO penetration depth used (8 km in blue, 10 km in green, 12 km in red, 16 km in cyan, and 20 km in magenta)

3.2.4 Success-Rate Analysis

In order to ascertain the success-rate of the calibration algorithm, a "failure to con-verge" condition was established. If the least-squares cost-function exceeded the num-ber of scan-angles used for calibration (200 for V-band channels, 40 for G-band chan-nels), the calibration result was rejected. The calibration success-rate versus channel is shown in Fig. 3-6.

Similar to previous results, the temperature sounding channels performed better than the water vapor channels, though all channels achieve at least 75% successful calibrations, or about 750 of the 1000 atmospheric profiles used in this study. There is also a general trend of higher success with deeper RO penetration.

3.2.5 Geographical Analysis

The locations of the rejected calibrations were examined for evidence of any geograph-ical bias or dependence. The locations of all 1000 profiles are shown along with all of the rejected calibrations for the worst performing case (207.4-GHz channel with a 20-km RO penetration depth) in Fig. 3-7. The locations of rejected cases are uniformly distributed around the globe, showing no obvious geographical correlations.

3.3 Discussion

The refractivity-to-brightness-temperature approximation performed poorly for the less-opaque channels, leading to errors being propagated into the calibrated results. However, it performed very well for the more opaque channels which showed the ability to achieve 0.25 K rms calibration error using the best-case RO penetration depth of 8-km, and 1.0 K rms error for the 20-km worst-case. These results are comparable to the <1.0 K radiometric accuracy shown for the current state-of-the-art ATMS instrument. The results from this study make the case that the proposed brightness temperature procedure, as outlined in section 2.1, may be suitable for use with channels in the 52-58 GHz temperature sounding band during the MiRaTA mission. Regarding GNSS-
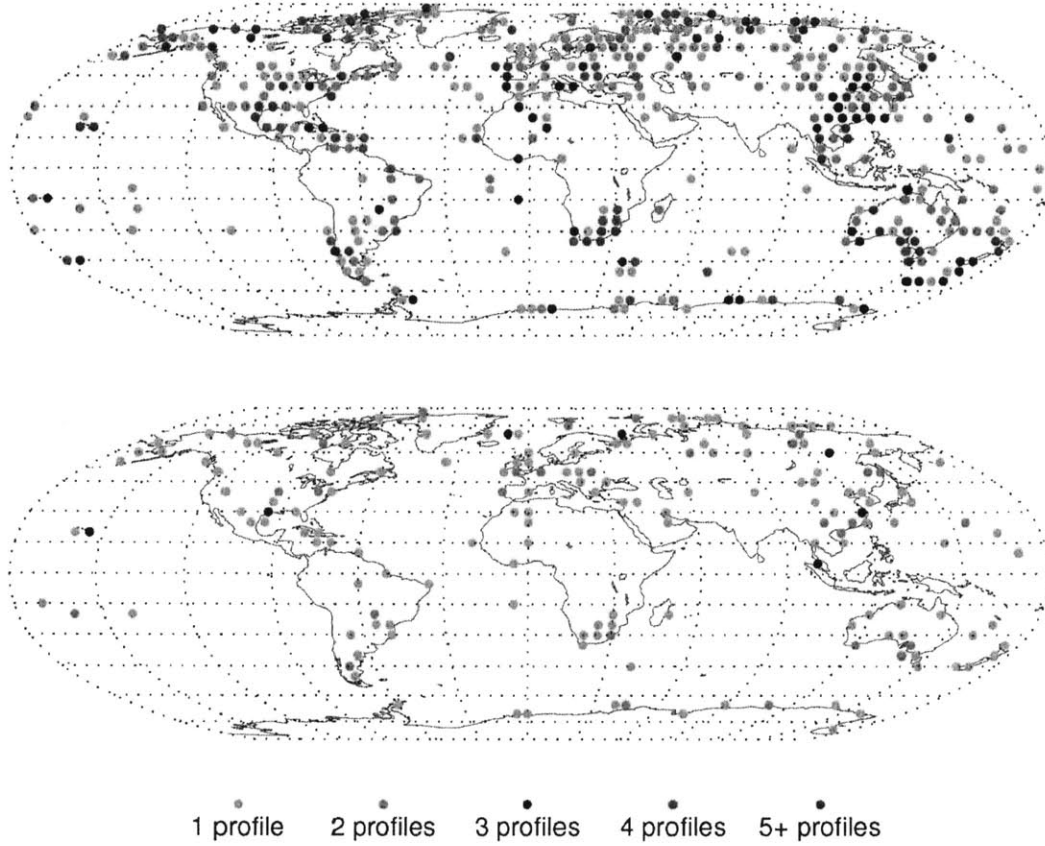
Figure 3-7: Geopgraphical locations of all 1000 profiles (top) and the rejected calibrations for the 207.4 GHz channel simulation using a 20 km RO penetration depth (bottom)

RO payload capability, lower RO penetration depths are desired, and thus receiver signal-to-noise ratio becomes an important design parameter.

Another promising result was the performance in retrieving the random angular offsets applied to the radiometer measurements. Across all of the channels and RO penetration depth simulations, the maximum error in angular offset retrieval was $<0.05°$, which can potentially be used to correct the attitude of the spacecraft. However, an important thing to note is that his improved pointing knowledge is only in the single axis of radiometer scan rotation.

Chapter 4

Parametric Sensitivity Studies

This chapter shows and discusses the results from the performance analyses focused on the sensitivity of the calibration method for a mission using the MicroMAS radiometer. Section 4.1 lists the key notes and assumptions that pertain to the results shown of this study. Section 4.2 shows the results of varying certain critical system design parameters and the impact on radiometer calibration. Section 4.3 provides some discussion of the results.

4.1 Key Notes and Assumptions

This study analyzes the sensitivity of the calibration algorithm performance with respect to varying system parameters, specifically the spacecraft altitude (section 4.2.1), radiometer beamwidth (section 4.2.2), and radiometer sampling rate (section 4.2.3). These three parameters were chosen because they all impact the microwave radiometer's ability to perform accurate limb-sensing for direct comparison with the RO measurements. The nominal system design has a spacecraft altitude of 500 km, a radiometer FWHM beamwidth of 2.4° , and a sampling rate of 2500 Hz. The pointing error is assumed to be perfect (0°), and the radiometer scan rate is assumed to be 1 Hz. In place of the ten channels used in the previous study, which represented the MiRaTa radiometer sounding bands, this study uses a single channel in the region of the 118 GHz oxygen-absorption band, similar to that used by the MicroMAS

radiometer. It is worth noting that this frequency band was not selected to optimize the calibration results. Instead, it is simply used as a common reference such that sensitivities and trends due to the calibration procedure can be determined for other system design parameters.

4.2   Results

4.2.1   Spacecraft Altitude

The first sensitivity study was performed on the spacecraft altitude, which affects the number of radiometer scan angles over which the limb is observed. The RMS error in the calibrated brightness temperature is shown in Fig. 4-1 as the altitude was varied between 300 km and 1100 km. Below 300 km altitude, small satellite orbits will decay quickly due to atmopsheric drag perturbations on the spacecraft, severely limiting the operational lifetime of the mission. Beyond 1100 km altitude, space environment becomes a hazard, as trapped radiation in the Van Allen belts can cause damage to on-board electronics.

The accuracy of the calibration algorithm degrades as the altitude increases, which is to be expected. As the orbiting altitude of the radiometer increases, the dynamic range of brightness temperatures across the limb gets collapsed into smaller windows of viewing angles with respect to the radiometer. For a fixed radiometer sample rate, this leads to fewer discrete scan-angles to observe, each with larger measurement uncertainties, causing larger calibration errors.

4.2.2   Radiometer Beamwidth

Another sensitivity study was performed on the beamwidth of the radiometer reflector, which affects the size of the beam angles used in the spatial averaging operation used to simulate radiometer brightness temperatures as a function of scan-angle. The RMS error in the calibrated brightness temperature is shown in Fig. 4-2 as the FWHM beamwidth was varied between 0.5° and 3.5 ° . For reference, the FWHM
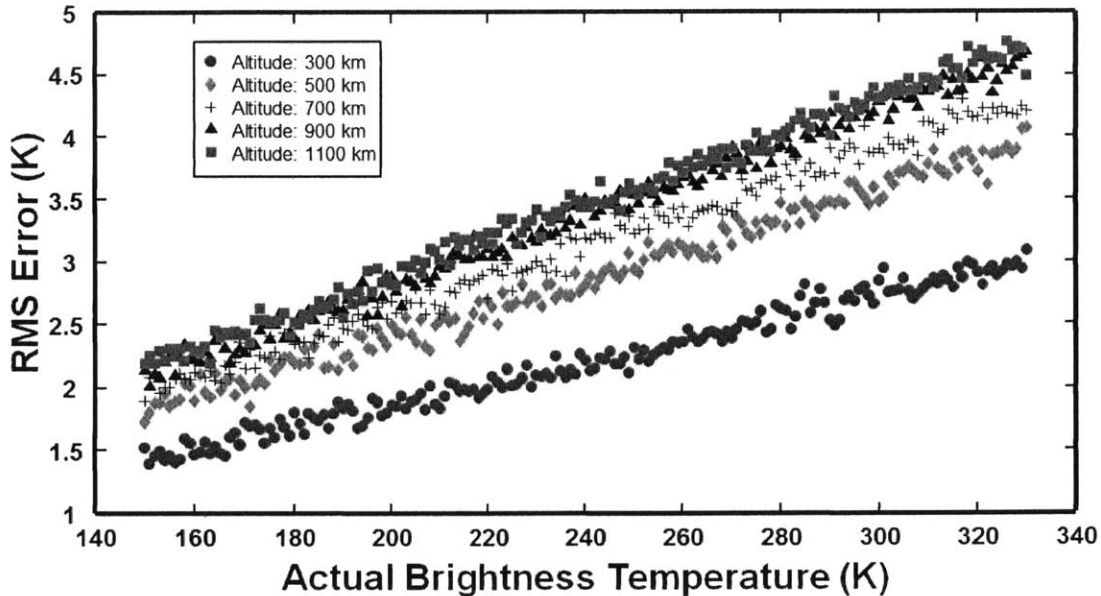
Figure 4-1: RMS error of calibrated brightness temperatures for varying the spacecraft altitude, assuming a 118 GHz radiometer

beamwidth of the MicroMAS radiometer is 2.4° .

Similar to the results for varying spacecraft altitude, the accuracy of the calibration algorithm degrades as the beamwidth increases. This is expected, as larger beam shapes would cause a larger range of brightness temperatures to be averaged into a given angle-discretized brightness temperature measurement, causing larger uncertainties in the limb measurements and thus larger calibration errors.

4.2.3 Radiometer Sampling Rate

The last sensitivity study was performed on the sampling rate of the radiometer, which affects the integration time in measuring brightness temperature. The resolution of brightness temperature measurements, ΔT, is inversely proportional to the integration time, τ, as expressed in the following equation [29]:

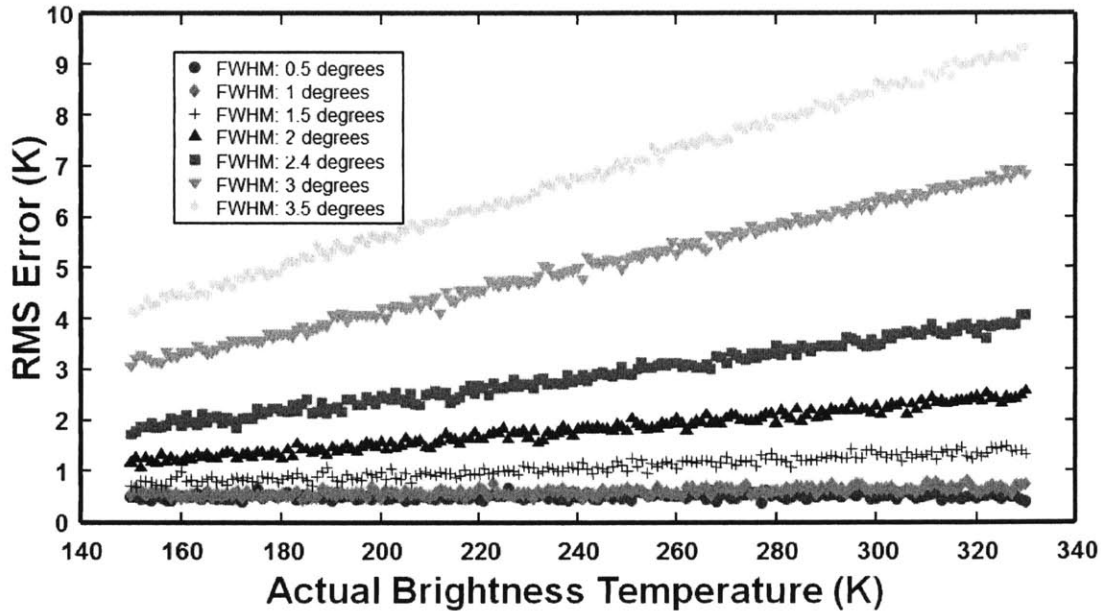$$\Delta T = \frac{T_{sys}}{\sqrt{B\tau}} \tag{4.1}$$

Figure 4-2: RMS error of calibrated brightness temperatures for varying the radiometer beamwidth, assuming a 118 GHz radiometer

where T_{sys} is the total system noise temperature, and B is the channel bandwidth.

Longer integration times effectively lower the system noise in order to increase the resolution of the brightness temperature measurement. However, integration time is also inversely proportional to the sampling rate. Therefore, increases in sampling rate should result in larger uncertainties in the radiometer measurements, causing larger calibration errors. The RMS error in the calibrated brightness temperature is shown in Fig. 4-3 as the FWHM beamwidth was varied between 2500 Hz and 20 kHz. As expected, the accuracy of the calibration algorithm degrades as the radiometer sampling rate is increased.

4.3 Discussion

Based on the results of this study, it is clear that the performance of the calibration procedure proposed in 2.1 is proportional to the system design parameters of orbital altitude, radiometer beamwidth, and radiometer sampling rate. These three
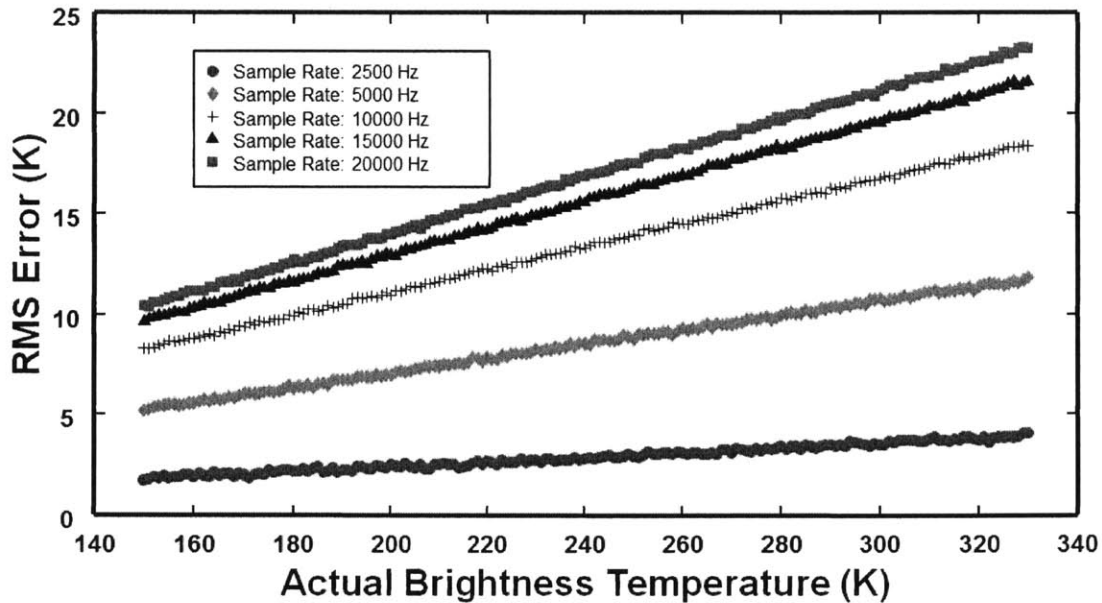
Figure 4-3: RMS error of calibrated brightness temperatures for varying the radiometer sampling rate, assuming a 118 GHz radiometer

parameters were chosen for their direct impact on the microwave radiometer's ability to sense the limb atmosphere within a reasonable resolution. The results from the three sensitivity studies agreed with expectations based on physical and geometrical principles.

The 118 GHz frequency used by MicroMAS does not seem to be as well-suited to achieving high-accuracy calibration as the 52-58 GHz frequencies used in the performance analyses in Chapter 3. However, these results can readily be compared against calibrated brightness temperatures computed using real CubeSat radiometer data once the MicroMAS satellite is deployed into orbit, and collocated data sets are found from RO databases.

Chapter 5

Conclusion

In summary, the authors have successfully analyzed the geometric and algorithmic opportunities in constructing a procedure for calibrating microwave radiometer brightness temperature measurements, such that it may be incorporated into a small-satellite constellation architecture capable of achieving dense, high-accuracy geospatial and temporal sampling of Earth radiances. The proposed calibration procedure involves the use of a GNSS radio occultation payload co-located on the same platform as the microwave radiometer, and a system design that allows for the radiometer to periodically sense the limb atmosphere. A simulation environment was developed in order to analyze the calibration procedure over 1000 global atmospheric profiles for accuracy, performance, and sensitivity. The calibration procedure was shown to achieve rms calibration errors as low as 0.25 K, assuming proposed system design parameters and assumed noise characteristics for the future MiRaTA validation mission to be launched in 2016. Parametric sensitivity studies showed that orbital altitude, radiometer bandwidth, and radiometer sampling rate have direct impact on the radiometer's ability to sense the limb atmopshere to a reasonable resolution, which in turn affects the calibration procedure.

With these results, there is a promising likelihood of success using this approach of calibrating microwave radiometers on future missions. However, consideration must be given to the system design for collecting collocated data between the two instruments. Further investigation into the approximations used between RO and

radiometer measurement profiles is recommended in order to include water vapor terms in addition to the temperature terms.

Bibliography

[1] Richard A. Anthes, P.A. Bernhardt, Y. Chen, L. Cucurull, K.F. Dymond, D. Ector, S.B. Healy, S-P Ho, D.C. Hunt, Y-H Kuo, et al. The COSMIC/FORMOSAT-3 Mission: early results. *Bulletin of the American Meteorological Society*, 89(3), 2008.

[2] Michael Bennett. Options for modernizing military weather satellites. In *Congressional Budget Office Working Paper Series 2012*, number 11, Washington, D.C., September 2012.

[3] Eric Berger. NOAA may cancel its participation in a critical satellite program. http://blog.chron.com/weather/2013/06/noaa-may-cancel-its-participation-in-a-critical-satellite-program/, June 2013.

[4] Rebecca Bishop, D.A. Hinkley, D.R. Stoffel, D.E. Ping, P.R. Straus, and T. Brubaker. First results from the GPS compact total electron content sensor (CTECS) on the PSSCT-2 nanosat. In *Proc. of the 26th Annual AIAA/USU Conference on Small Satellites*, number SSC12-XI-2, Logan, UT, August 2012.

[5] William J Blackwell, Laura J Bickmeier, Laura G Jairam, and R Vincent Leslie. On-orbit radiometric validation and field-of-view calibration of spaceborne microwave sounding instruments. In *Asia-Pacific Remote Sensing*, pages 71540A–71540A. International Society for Optics and Photonics, 2008.

[6] William J Blackwell, Laura J Bickmeier, R Vincent Leslie, Michael L Pieper, Jenna E Samra, Chinnawat Surussavadee, and Carolyn A Upham. Hyperspectral microwave atmospheric sounding. *Geoscience and Remote Sensing, IEEE Transactions on*, 49(1):128–142, 2011.

[7] William J. Blackwell and et al. Nanosatellites for Earth environmental monitoring: the MicroMAS project. In *Proc. of the 26th Annual AIAA/USU Conference on Small Satellites*, number SSC12-I-2, Logan, UT, August 2012.

[8] William J. Blackwell and et al. MicroMAS: a first step towards a nanosatellite constellation for global storm observation. In *Proc. of the 27th Annual AIAA/USU Conference on Small Satellites*, number SSC13-XI-1, Logan, UT, August 2013.

55

[9] W.J. Blackwell, R. Bishop, K. Cahoy, B. Cohen, C. Crail, L. Cucurull, P. Dave, M. DiLiberto, N. Erickson, C. Fish, S. Ho, R.V. Leslie, A.B. Milstein, and I.A. Osaretin. Radiometer calibration using colocated gps radio occultation measurements. *Geoscience and Remote Sensing, IEEE Transactions on*, PP(99):1–11, 2014.

[10] W.J. Blackwell, M. DiLiberto, R.V. Leslie, A. Milstein, I. Osaretin, B.S. Cohen, P.K. Dave, and K. Cahoy. Earth limb calibration of scanning spaceborne microwave radiometers. In *Geoscience and Remote Sensing Symposium (IGARSS), 2013 IEEE International*, pages 1934–1935, July 2013.

[11] Eric S. Blake, Todd B. Kimberlain, Robert J. Berg, J.P. Cangialosi, and John L. Beven II. Tropical cyclone report: Hurricane Sandy. *National Hurricane Center*, 12, 2013.

[12] Shannon T. Brown, Shailen Desai, Wenwen Lu, and Alan B. Tanner. On the long-term stability of microwave radiometers using noise diodes for calibration. *Geoscience and Remote Sensing, IEEE Transactions on*, 45(7):1908–1920, 2007.

[13] Austin Satellite Design. Dual frequency reprogrammable software-defined gps receiver for cubesats. http://austinsat.net/ dual-frequency-reprogrammable-software-defined-gps-receiver-for-cubesats/, May 2014.

[14] Danny Gale, B. French, M. Perez, and J. Haynes. Polarcube: All-star as a platform for passive radiometric sensing. In *2012 COSGC Space Research Symposium*, April 2012.

[15] Yong Han and E.R. Westwater. Analysis and improvement of tipping calibration for ground-based microwave radiometers. *Geoscience and Remote Sensing, IEEE Transactions on*, 38(3):1260–1276, May 2000.

[16] Shu-peng Ho, Xinan Yue, Zhen Zeng, Chi O. Ao, Ching-Yuang Huang, Emil R. Kursinski, and Ying-Hwa Kuo. Applications of COSMIC radio occultation data from the troposphere to ionosphere and potential impacts of COSMIC-2 data. *Bulletin of the American Meteorological Society*, 95(1):ES18–ES22, January 2014.

[17] Edward Kim, Cheng-Hsuan J. Lyu, Kent Anderson, R. Vincent Leslie, and William J. Blackwell. S-npp atms instrument prelaunch and on-orbit performance evaluation. *Journal of Geophysical Research: Atmospheres*, pages 1–18, 2014.

[18] E.R. Kursinski, G.A. Hajj, J.T. Schofield, R.P. Linfield, and K.R. Hardy. Observing Earth's atmosphere with radio occultation measurements using the Global Positioning System. *Journal of Geophysical Research: Atmospheres (1984–2012)*, 102(D19):23429–23465, 1997.

[19] Florian Ladstadter. Collocating GRAS with nadir sounders onboard of Metop: an assessment for instrument and climate monitoring. In *GRAS SAF CDOP Visiting Scientists*, number VS7, March 2012.

[20] Boon Lim, M. Shearn, D. Dawson, C. Parashare, A. Romero-Wolf, D. Russell, and J. Steinkraus. Development of the radiometer atmospheric cubesat experiment payload. In *Geoscience and Remote Sensing Symposium (IGARSS), 2013 IEEE International*, pages 849–851, July 2013.

[21] David Malakoff. Warning Issued for Looming Data Gap From Fleet of Weather Satellites. *Science*, 339:895–895, February 2013.

[22] Anne Marinan. From CubeSats to constellations : systems design and performance analysis. Master's thesis, Massachusetts Institute of Technology, Department of Aeronautics and Astronautics, September 2013.

[23] Tony McNally, Massimo Bonavita, and Jean-Noël Thépaut. The role of satellite data in the forecasting of Hurricane Sandy. *Monthly Weather Review*, 142(2), 2014.

[24] NOAA. Study shows polar-orbiting satellite data was key to pinpointing Sandy's track and time of landfall. http://www.noaanews.noaa.gov/stories2012/20121211_poesandsandy.html, December 2012.

[25] NASA OIG Office of Audits. NASA's management of the NPOESS Preparatory Project. In *NASA Office of Inspector General Audit Reports*, number IG-11-018, June 2011.

[26] WMO OSCAR. Capability: MW temperature/humidity sounding from LEO. http://www.wmo-sat.info/oscar/observingmissions/view/5, May 2014.

[27] C+ Rocken, R Anthes, M Exner, D Hunt, S Sokolovskiy, R Ware, M Gorbunov, W Schreiner, D Feng, B Herman, et al. Analysis and validation of gps/met data in the neutral atmosphere. *Journal of Geophysical Research: Atmospheres (1984-2012)*, 102(D25):29849–29866, 1997.

[28] Philip Rosenkranz. *Absorption of microwaves by atmospheric gases*. Atmospheric Remote Sensing by Microwave Radiometry. John Wiley and Sons.

[29] Neils Skou. *Microwave radiometer systems: design and analysis*. Artech House, Norwood, MA, second edition, 2006.

[30] A Von Engeln, S Healy, Ch Marquardt, Y Andres, and F Sancho. Validation of operational gras radio occultation data. *Geophysical Research Letters*, 36(17), 2009.

[31] A. Wallard and W. Zhang. Measurement challenges for global observation systems for climate change monitoring: Traceability, stability and uncertainty. In *IOM Report*, number 105, April 2010.

[32] Xiaolei Zou, Lin Lin, and Fuzhong Weng. Absolute calibration of ATMS upper level temperature sounding channels using GPS RO observations. 2014.